Generalized Spatio-Chromatic Diffusion

Giuseppe Boccignone, *Member*, *IEEE*, Mario Ferraro, and Terry Caelli, *Fellow*, *IEEE*

Abstract—In this paper, a framework for diffusion of color images is presented. The method is based on the theory of thermodynamics of irreversible transformations which provides a suitable basis for designing correlations between the different color channels. More precisely, we derive an equation for color evolution which comprises a purely spatial diffusive term and a nonlinear term that depends on the interactions among color channels over space. We apply the proposed equation to images represented in several color spaces, such as RGB, CIELAB, Opponent colors, and IHS.

Index Terms—Color images, scale-space, vector-valued diffusion.

1 Introduction

Even though color information is essential to many vision tasks, most biological and computational vision models work exclusively in the luminance domain. As a consequence, research has been focused mainly on sources of information such as intensity gradients, textural features, or geometrical cues. However, data from biological vision systems show that boundary representations do not segregate achromatic and chromatic signals into different representations but, rather, they pool signals from all chromatic and achromatic sources in order to generate the most accurate boundaries possible in response to any given stimulus array [1]. Interestingly, a firm theoretical basis for such a claim has been provided by computer vision [2]. Namely, it has been shown that the effectiveness of different edge operators, as theoretically measured by Chernoff information, can improve by using either multiscale processing and chromaticity in addition to gray scale. However, these results leave open the very issue of how to combine, in a single representation, multiscale processing and color. In computer vision, multiscale representations of a gray-level image I have been obtained by fine-to-coarse transformations that can be modeled, in general, by a diffusion or heat equation [3], [4],

$$\partial_t I = D\nabla^2 I, \tag{1}$$

where D is the diffusivity or conductance, a constant which, without loss of generality, is usually set equal to 1, ∂_t denotes the partial derivative $\partial/\partial t$ and ∇^2 is the Laplacian operator. A vast amount of research on diffusion processes can be found in the computer and computational vision literature mostly devoted to monochromatic images (for an in depth treatment, see [5], [6], [7]).

A vector-valued (multivalued) image is a smooth mapping from the image domain $\Omega \subseteq \mathbf{R}^2$ to an m-dimensional range, $\mathbf{I}: \Omega \to \mathbf{R}^m$; in other terms, it is a set of single-valued images, or channels, sharing the same domain, i.e., $\mathbf{I}(\mathbf{r}) = (I_i(\mathbf{r}))^T$, where $i = 1, \dots, m$ and $\mathbf{r} = (x, y)$ denotes a point in Ω. A color image can be considered a vector-valued image of three components ($m = 3$) or color channels.

A number of authors [8], [9], [10], [11] have addressed vector-valued diffusion by extending to $\mathbf{R}^m$ scalar anisotropic diffusion schemes ([6], [12]). For instance, Whitaker and Gerig [8] obtain vector-valued anisotropic diffusion through a system of single-valued diffusion processes, evolving simultaneously but sharing a common conductance modulating term d, namely, $\partial_t I_i = \nabla \cdot (d(\|\mathcal{J}\|)\nabla I_i)$, where $\|\mathcal{J}\|$ is the Euclidean norm of the generalized Jacobian matrix of $\mathbf{I}$ (for notational convenience, we simply write $I_i(\mathbf{r})$ as I_i). Analogously, Weickert [9] proposes a common conductance d which takes into account information from all channels as a function of the structure tensor for vector images, $M_\rho(\nabla \mathbf{I}_\sigma) = \sum_{i=1}^m M_\rho(\nabla I_{i,\sigma})$, where $M_\rho(\nabla I_{i,\sigma}) = K_\rho * (\nabla I_{i,\sigma} \nabla I_{i,\sigma}^T)$ is the scalar structure tensor or second-moment matrix, K_ρ being a Gaussian kernel, ρ and σ the integration and noise scales, respectively, ($\rho \gg \sigma$). The function d is designed to allow maximal smoothing along a coherence direction determined via the eigenvector corresponding to the smallest eigenvalue of the structure tensor. A different approach has been proposed in [10] by considering color images as surfaces. In this case, transitions from fine to coarse scale of resolution can be generated by a suitable choice of the metric tensor. In particular, the so-called Beltrami flow is governed by the equation

$$\partial_t I_i = \frac{1}{g^{1/2}} \sum_{\mu=1}^{2} \frac{\partial}{\partial x_\mu} \left(g^{1/2} \sum_{\nu=1}^{2} g^{\mu\nu} \frac{\partial}{\partial x_\nu} I_i \right),$$

where $x_1 = x$, $x_2 = y$, $g^{\mu\nu}$ is the metric tensor and g is its determinant. In a similar vein, Sapiro and Ringach [11] choose d as a decreasing function of $(\lambda_+ - \lambda_-)$, where λ_+ and λ_- are the eigenvalues of the metric tensor and diffusion is constrained to occur normal to the direction of maximal change. Interestingly, all such anisotropic models relax, in the

- G. Boccignone is with the Dipartimento di Ingegneria dell'Informazione e Ingegneria Elettrica and National Institute for the Physics of Matter, Universitá di Salerno, via Ponte Don Melillo 1, 84084 Fisciano (SA), Italy. E-mail: boccig@unisa.it.
- M. Ferraro is with the Dipartimento di Fisica Sperimentale and National Institute for the Physics of Matter, Universitá di Torino, via Giuria 1, 10125 Torino, Italy. E-mail: ferraro@ph.unito.it.
- T. Caelli is with the Department of Computing Science, University of Alberta, General Services Building, Edmonton, Alberta, Canada T6G 2H1. E-mail: tcaelli@ualberta.ca.

Manuscript received 19 Jan. 2001; revised 5 Dec. 2001; accepted 26 Mar. 2002.
Recommended for acceptance by H. Christensen.
For information on obtaining reprints of this article, please send e-mail to: tpami@computer.org, and reference IEEECS Log Number 113511.

isotropic limit, to a system of single-valued, scalar partial differential equations (PDEs), each taking place on a separate channel I_i, with $\partial_t I_i = \nabla^2 I_i$ (Independent Channel Diffusion (ICD)). For instance, the Laplace-Beltrami operator reduces to the ordinary Laplacian when g is the Euclidean metric.

Here, a different perspective to the problem is presented, founded on the concept of color channel interactions in the framework of the thermodynamics of open systems. It will be shown that, by considering the different channels as interacting systems, a generalized diffusion equation can be derived that determines the evolution in spatio-chromatic scale space, (Generalized Spatio-Chromatic Diffusion (GSCD)), without being constrained by a particular form of diffusivity. As a result, the evolution equation across scales comprises a purely diffusive term and a nonlinear term that depends on the interactions between channels. In this respect, our approach shares some common aspects either with other approaches, that derive systems of diffusion equations in a variational framework, for instance [13], [14], the latter being specifically conceived for chromaticity diffusion, or with pseudolinear scale-spaces recently introduced by Florack [15]. The proposed diffusion scheme is intended mainly to provide a preprocessing step to later specialized stages of visual analysis; meanwhile, as it will be shown in the sequel, it exhibits appreciable noise suppression properties. Also, a possible anisotropic extension of GSCD will be discussed.

2 Generalized Diffusion

We consider scale parametrized color images, which we denote by $\mathbf{I}(\mathbf{r}, t) = (I_i(\mathbf{r}, t))^T$, where the index $i = 1, .., m$, defines the ith color channel and t is the scale of resolution: Small values of t correspond to fine scales, while large values correspond to coarse scales. A transformation from one scale to another is given by an operator $\mathcal{T}$ that takes the original image $\mathbf{I}(\cdot, 0)$ to an image at a scale t, namely, $\mathcal{T}_t : \mathbf{I}(\cdot, 0) \rightarrow \mathbf{I}(\cdot, t)$. We assume $\mathcal{T}$ to be a *semidynamical system*, that is, a semigroup of transformations for which $\mathcal{T}_{t+t^0}\mathbf{I}(\cdot, 0) = \mathcal{T}_t(\mathcal{T}_{t^0}\mathbf{I}(\cdot, 0)) = \mathcal{T}_{t^0}\mathbf{I}(\cdot, t), \mathcal{T}_0\mathbf{I}(\cdot, t) = \mathbf{I}(\cdot, t)$, where $t \in \mathbf{R}^+$. The characterization of $\mathcal{T}$ as a semidynamical system ensures that it is a *noninvertible* or *irreversible* transformation which cannot be run backward across scale. A transformation $\mathcal{T}$ can be implemented implicitly through a differential equation and the diffusion equation has been widely used in this context; then, it would be tempting to adapt this kind of approach to the case of color images. Most anisotropic, vector-valued models simplify, in the case of an isotropic process, to ICD, i.e., a system of single-valued diffusion processes evolving simultaneously:

$$\partial_t I_i = \nabla^2 I_i. \tag{2}$$

Unfortunately, the system specified by (2) does not allow interactions among different color channels to take place, whereas there is a general agreement [8], [11], [9], [13], [14], [15], [16], [17] that the processing and interpretation of color images cannot be reduced to the separate processing of three independent channels, but must account, to some extent, for dependencies between channels, whatever the channels employed.

Conceptualizations of color diffusion image models can gain from physical metaphors. In physics, there are many instances in which different systems interact with each other. This is the case, for instance, of thermodynamics of open systems, where different thermodynamical systems exchange energy or matter [18]. In such cases, the equations determining the evolution of the processes under observation must take into account the interactions among different systems and then they have a more complex form than for isolated systems. For example, consider diffusion of heat: if the system is isolated the evolution of the temperature T is governed by a diffusion equation, similar to (1) whereas in case of an open system a more general equation holds, namely,

$$\partial_t T = -div\vec{J}, \tag{3}$$

where $\vec{J}$ is the heat flow [18]. Note that by setting $\vec{J} = -D\nabla T$, where ∇ is the gradient operator, one obtains $\partial_t T = D\nabla^2 T$, the usual diffusion equation. Analysis of thermodynamical open systems is usually very complex; fortunately, it is known that, for a large class of transformations, flows can be thought of as driven by *generalized thermodynamical forces* of which they are linear functions. For instance, Fourier's law states that heat flow is linearly dependent from the gradient of the temperature. In general, in the linear regime, $\vec{J} = L\vec{X}$ [18], where $\vec{X}$ is the generalized force and is of the nature of a gradient and L is a matrix of *phenomenological coefficients* [18] not depending on either $\vec{X}$ or $\vec{J}$. Indeed, this cause-effect relation between $\vec{X}$ and $\vec{J}$, which is reminiscent of the connection between force and acceleration in Newtonian mechanics, renders it plausible to call $\vec{X}$ a thermodynamical force.

To apply this formalism to color images, any color channel will be considered as an open system interacting with the others. Then, for each color channel, the transition from fine to coarse scales can be modeled through the equation

$$\partial_t I_i = -div\vec{J}_i, \tag{4}$$

(compare (3)). In turn, for each i, the flow is given by $\vec{J}_i = \sum_{j=i}^m L_{ij}\vec{X}_j$.

In order to model interactions, one has to choose generalized forces $\vec{X}_i$ and coefficients L_{ij}. In thermodynamics, there is some freedom in choosing generalized forces provided that the resulting equations be consistent with those that hold for isolated systems. In particular, for heat diffusion $\vec{X} = \nabla(1/T)$ [18]; then, in our treatment, the corresponding form is $\vec{X}_i = \nabla(1/I_i)$. This choice of $\vec{X}_i$ is consistent with the definition of the thermodynamic theory, which we use to shape color channel interactions and, more importantly, when applied to monochromatic images, that can be considered as isolated systems, reproduces known results [19]. As for the coefficients L_{ij}, Onsager's reciprocity principle must hold [18], namely, $L_{ij} = L_{ji}$. In this case, this simply assumes that we make no prior assumptions about biases in the coupling between color channels. In addition, if there are no interactions among channels, (4) must become ICD equation (2). Define $L_{ij} = \chi_{ij} f(I_i, I_j)$, where $\chi_{ij} = \chi_{ji}$ are symmetric coefficients between channels i and j whose maximum value is $\chi_{ii} = 1$; in case of independent channels $\chi_{ij} = \delta_{ij}$. Next, it will be shown that, under these conditions, the function f must satisfy the relation

$$f(I_i, I_i) = I_i^2. \tag{5}$$

By inserting $\vec{J}_i = \sum_{j=i}^{n} L_{ij}\vec{X}_j$ into (4),

$$\partial_t I_i = -div\left(\sum_j L_{ij}\vec{X}_j\right) = \sum_j \nabla \cdot \left(\chi_{ij} f(I_i, I_j)\frac{\nabla I_j}{I_j^2}\right); \quad (6)$$

if $\chi_{ij} = \delta_{ij}$, the equation is simply $\partial_t I_i = \nabla \cdot \left(f(I_i, I_i)\frac{\nabla I_i}{I_i^2}\right)$, which can also be written as

$$\partial_t I_i = \frac{f}{I_i^2}\nabla^2 I_i + \frac{1}{I_i^2}\nabla f(I_i, I_i)\cdot \nabla I_i - \frac{2f}{I_i^3}(\nabla I_i)^2.$$

This equation is the same as (2), if

$$\frac{f}{I_i^2}\nabla^2 I_i = \nabla^2 I_i, \quad \frac{1}{I_i^2}\nabla f(I_i, I_i)\cdot \nabla I_i - \frac{2f}{I_i^3}(\nabla I_i)^2 = 0. \quad (7)$$

The first part of (7) holds if and only if $f(I_i, I_i) = I_i^2$. Next, it is straightforward to check that, if $f(I_i, I_i) = I_i^2$, the second equation is automatically satisfied. Thus, the simplest form for f satisfying (5) is then $f(I_i, I_j) = I_i I_j$ and we have chosen to study couplings of the form $L_{ij} = \chi_{ij} I_i I_j$.

By using (6), we obtain the following system of coupled evolution equations

$$\partial_t I_i = \sum_j \nabla \cdot \left(\chi_{ij} I_i I_j \frac{\nabla I_j}{I_j^2}\right),$$

that, after some computations, becomes:

$$\begin{aligned}\partial_t I_i = &\nabla^2 I_i + \sum_{j\neq i}\chi_{ij}\left(\frac{I_i}{I_j}\nabla^2 I_j + \frac{1}{I_j^2}\left(I_j\left(\partial_x I_i \partial_x I_j + \partial_y I_i \partial_y I_j\right)\right.\right.\\ &\left.\left.- I_i\left(\partial_x I_j \partial_x I_j + \partial_y I_j \partial_y I_j\right)\right)\right).\end{aligned} \quad (8)$$

This set of PDEs can be written in matrix form as:

$$\begin{aligned}\partial_t I_i = &\nabla^2 I_i + \sum_{j\neq i}\chi_{ij}\frac{I_i}{I_j}\nabla^2 I_j\\ &+ \sum_{j\neq i}\frac{\chi_{ij}}{I_j^2}\begin{bmatrix} I_j \\ -I_i\end{bmatrix}^T \begin{bmatrix}\partial_x I_i & \partial_y I_i \\ \partial_x I_j & \partial_y I_j\end{bmatrix}\begin{bmatrix}\partial_x I_j \\ \partial_y I_j\end{bmatrix}.\end{aligned} \quad (9)$$

Because of the nonlinear interactions occurring between channels, the average gray level of each channel needs not to be preserved. In this sense, the behavior of each PDE has qualitative relation to affine scale spaces, based on Gaussian kernels with arbitrary covariance matrices [20], [21]. Here, smoothing control in each channel is provided by the other channels. The system of equations (9) can be written in a more compact form which also makes clearer the meaning of the different terms. For a given index i, denoting the channel under consideration and for each $j \neq i$, define $h_{ij} = \chi_{ij}\frac{I_i}{I_j}$,

$$\vec{w}_{ij}^T = \frac{\chi_{ij}}{I_j^2}\begin{bmatrix} I_j \\ -I_i\end{bmatrix}^T;$$

denote by $\vec{v}_j$ the gradient $\left[\partial_x I_j, \partial_y I_j\right]$ of the channel j and, finally, define the vector field $\vec{u}_{ij} = \left[I_i, I_j\right]$. Then,

$$\begin{bmatrix}\partial_x I_i & \partial_y I_i \\ \partial_x I_j & \partial_y I_j\end{bmatrix}$$

is the Jacobian matrix $D\vec{u}_{ij}$ and, hence,

$$\begin{bmatrix}\partial_x I_i & \partial_y I_i \\ \partial_x I_j & \partial_y I_j\end{bmatrix}\begin{bmatrix}\partial_x I_j \\ \partial_y I_j\end{bmatrix}$$

is the derivative of $\vec{u}_{ij}$ in the direction $\vec{v}_j$, i.e., $\nabla_{\vec{v}_j}\vec{u}_{ij}$. In conclusion, (9) takes the form

$$\partial_t I_i = \nabla^2 I_i + \sum_{j\neq i}\left[h_{ij}\nabla^2 I_j + \vec{w}_{ij}^T \nabla_{\vec{v}_j}\vec{u}_{ij}\right]. \quad (10)$$

Then, GSCD equations comprise a purely diffusive term and a nonlinear term that depends on the interactions among channels. The first term, $\nabla^2 I_i$, is the Laplacian accounting for isotropic diffusion within the channel i under consideration. The second term is due to interaction among channels: The Laplacian $\nabla^2 I_j$ represents diffusion weighted by h_{ij}, taking place in the channel j, while $\nabla_{\vec{v}_j}\vec{u}_{ij}$ gauges the effect of the rate of change of the field $\vec{u}_{ij}$, along $\vec{v}_j$. Using a vector notation, the system (10) can be written as

$$\partial_t \mathbf{I} = \nabla^2 \mathbf{I} + F(\mathbf{I}). \quad (11)$$

The vector equation (11) can be considered a particular type of reaction-diffusion (R-D) system of equations, where $\nabla^2 \mathbf{I}$, is the diffusion term, whereas the nonlinear reaction term $F(\mathbf{I}) = F\left(I_i, I_j\right)$ is given by $\sum_{j\neq i}[h_{ij}\nabla^2 I_j + \vec{w}_{ij}^T \nabla_{\vec{v}_j}\vec{u}_{ij}]$. In this sense, GSCD is related to pseudolinear scale-spaces which appear to provide natural multiscale representations in the context of early vision, as they potentially account for nonlinearities that are essential when dealing with vector-valued images [15]. R-D systems of equations are known to generate patterns, that is, spatially nonuniform states [22]; in our case, these states correspond to nonuniform color intensities in the three channels. In some sense, since R-D equations preserve and enhance structures (cf. Fig. 8), they seem to share some properties of anisotropic diffusion [12]. Systems of equations of the reaction-diffusion type have been derived, from the theory of variations, and used in studies of evolution of either monochromatic images at different scales [23] or vector-valued images [14], [13]. For instance, Proesmans et al. [13] have discussed in detail a principled way to design a system of anisotropic diffusion equations to be used in multispectral analysis (briefly PPV method). Their equations have been obtained by introducing a Perona-Malik nonlinearity [24] in a system of R-D equations derived via a variational approach, which then reads

$$\begin{aligned}\partial_t \mathbf{I} &= c(\gamma)\nabla^2 \mathbf{I} + V(v, \gamma)\\ \partial_t \rho &= \rho \nabla^2 v + \Phi(\gamma)\\ \partial_t \gamma &= \xi \nabla^2 \gamma + G(\mathbf{I}),\end{aligned} \quad (12)$$

where v, γ are the coupling parameters, ρ and ξ are tunable numerical parameters. In particular, $G(\mathbf{I}) = G(\max(\nabla\|I_R\|, \nabla\|I_G\|, \nabla\|I_B\|))$ ensures the coupling among the different RGB channel gradients [13].

In order to provide an anisotropic extension of GSCD system of equations (briefly GSCAD) and to compare it to PPV method, we rewrite Onsager's coefficients L_{ij}, that modulate the thermodynamical forces $\vec{X}_j$, as $L_{ij} = g\chi_{ij} f(I_i, I_j)$. Here, g is a variable conductance function which, like Perona-Malik's, is a nonnegative, monotonically decreasing function of the magnitude of local image gradients in channels I_i and I_j; namely, $g = g\big(\varphi_{ij}(\|\nabla I_i\|, \|\nabla I_j\|)\big)$, where $\varphi_{ij}(\cdot)$ is a suitable combination function; further, to be consistent with Onsager's reciprocity conditions we assume $\varphi_{ij} = \varphi_{ij}$. There are several possible choices of $\varphi_{ij}(\cdot)$: Here, to allow comparisons between GSCAD and PPV, we use $\varphi_{ij} = \max(|\nabla I_i|, |\nabla I_j|)$. Note that, if $i = j$, $g = g(\|\nabla I_i\|)$, thus reducing (11) to a system of Perona-Malik equations independently applied to each channel. By inserting the modified L_{ij} coefficients in (6), the general case can be obtained as $\partial_t I_i = g\nabla^2 I_i + \sum_{j\neq i} g[h_{ij}\nabla^2 I_j + \vec{w}_{ij}^T \nabla_{\vec{v}_j}\vec{u}_{ij}]$ or, in R-D form,

$$\partial_t \mathbf{I} = g\nabla^2 \mathbf{I} + F(\mathbf{I}, g). \tag{13}$$

Some differences must be noted between the PPV system and GSCAD: As remarked, the approaches used to derive the equations were very different, namely, a variational approach and a thermodynamical framework, respectively; moreover, our approach seems to be more economical from a computational point of view in that it employs a system of three scalar differential equations versus five differential equations (compare (13) and (12)).

3 Experiments

Different color spaces can be used to deal with color images, there is a variety of spaces and no theoretical method has been developed to choose the most appropriate with respect to a problem at hand; the number of variables involved in practical applications makes such choice unfeasible. For this reason, we have not restricted our analysis to a specific space, but rather, we have carried out experiments in a variety of spaces.

3.1 Color Spaces and Transforms

A color space is a geometrical and mathematical representation of color and there is a variety of such representation either derived from hardware considerations (e.g., RGB, YCrCb, NTSC, YIQ, CMYK, etc.), or colorimetry issues (e.g., XYZ, UCS, CIELAB, CIELUV), or visual perception motivations (Opponent colors, IHS, HSV, etc.) A survey can be found in [25], [26], [27]. We will consider, as representative of such three classes of spaces, RGB, CIELAB, Opponent, and IHS.

The original RGB (red, green, blue) color space is widely used to represent image data, primarily due to the availability of such data as produced, for instance, by a color video camera which analyzes the collected light with three broadband filters transmitting in the red, green, and blue regions of the spectrum. Formally, this process generates a 3D vector $\mathbf{I}_{RGB}(\mathbf{r}) = (R(\mathbf{r}), G(\mathbf{r}), B(\mathbf{r}))^T$ for each pixel, where each component has a value ranging from 0 to 255. All of the color spaces described below are mathematical transformation based on this original RGB data. The CIE 1976 color space, abbreviated CIELAB, is a uniform color space defined by CIE (Commission Internationale de l'Eclairage) for use in colorimetry. It is based on the intermediate CIE XYZ tristimulus space derived from RGB as follows [26]:

$$\begin{aligned} X(\mathbf{r}) &= 0.41245\widehat{R}(\mathbf{r}) + 0.35758\widehat{G}(\mathbf{r}) + 0.18042\widehat{B}(\mathbf{r}) \\ Y(\mathbf{r}) &= 0.21267\widehat{R}(\mathbf{r}) + 0.71516\widehat{G}(\mathbf{r}) + 0.07217\widehat{B}(\mathbf{r}) \\ Z(\mathbf{r}) &= 0.01933\widehat{R}(\mathbf{r}) + 0.11919\widehat{G}(\mathbf{r}) + 0.95023\widehat{B}(\mathbf{r}), \end{aligned} \tag{14}$$

where the triplet $(\widehat{R}, \widehat{G}, \widehat{B})$ is the normalized version of (R, G, B), and takes values in the $[0, 1]$ range. The CIELAB equation is then applied to the tristimulus values to obtain the CIELAB vector $\mathbf{I}_{Lab}(\mathbf{r}) = (L^*(\mathbf{r}), a^*(\mathbf{r}), b^*(\mathbf{r}))^T$,where L^* represents an achromatic lightness value, a^* and b^* two chromatic values,

$$\begin{aligned} L^*(\mathbf{r}) &= 116f(Y(\mathbf{r})/Y_n) - 16 \\ a^*(\mathbf{r}) &= 500[f(X(\mathbf{r})/X_n) - f(Y(\mathbf{r})/Y_n)] \\ b^*(\mathbf{r}) &= 200[f(Y(\mathbf{r})/Y_n) - f(Z(\mathbf{r})/Z_n)]. \end{aligned} \tag{15}$$

Here, X_n, Y_n, Z_n are the tristimuli of a reference "white stimulus" as defined by a CIE standard illuminant, D65, in this case, and are obtained setting $\widehat{R} = \widehat{G} = \widehat{B} = 1$. Function f reads

$$f(q) = \begin{cases} q^{1/3}, & \text{when } q > 0.008856 \\ 7.787q + \frac{16}{116}, & \text{when } q \leq 0.008856, \end{cases} \tag{16}$$

where $q \in \{X/X_n, Y/Y_n, Z/Z_n\}$. The Opponent color model argues for the existence of three channels produced by linear combinations of the RGB channels. More precisely, we have used the Opponent color space as defined in [25], that is, $\mathbf{I}_{Opp}(\mathbf{r}) = (WB(\mathbf{r}), RG(\mathbf{r}), BY(\mathbf{r}))^T$, where

$$\begin{aligned} WB(\mathbf{r}) &= R(\mathbf{r}) + G(\mathbf{r}) + B(\mathbf{r}) \\ RG(\mathbf{r}) &= R(\mathbf{r}) - G(\mathbf{r}) \\ BY(\mathbf{r}) &= 2B(\mathbf{r}) - R(\mathbf{r}) - G(\mathbf{r}). \end{aligned} \tag{17}$$

WB represents light-dark variations, whereas RG and BY are called the opponent colors, and denote the red-green and blue-yellow hue pairs, respectively. The IHS system is a simplified version of the Munsell system. The I component, *intensity*, corresponds roughly to the brightness of the signal. The H component, *hue*, is approximately proportional to the wavelength of the color. The S component, *saturation*, measures the amount of white that is in the color (e.g., pink is an unsaturated red). This space can be modeled mathematically in polar coordinates, where the *hue* is specified by the angle, *saturation* as radial component, and *intensity* vertical to hue/saturation plane. More precisely, the conversion from the RGB color space to IHS is done in two steps [27]. First, the RGB coordinates are rotated to form the coordinate system (IV_1V_2) whose axis is the line $R = G = B$:

$$\begin{aligned} I(\mathbf{r}) &= \sqrt{3}/3R(\mathbf{r}) + \sqrt{3}/3G(\mathbf{r}) + \sqrt{3}/3B(\mathbf{r}) \\ V_1(\mathbf{r}) &= 1/\sqrt{2}G(\mathbf{r}) - 1/\sqrt{2}B(\mathbf{r}) \\ V_2(\mathbf{r}) &= 2/\sqrt{6}R(\mathbf{r}) - 1/\sqrt{6}G(\mathbf{r}) - 1/\sqrt{6}B(\mathbf{r}). \end{aligned} \tag{18}$$

Then, the rectangular coordinates (V_1V_2) are transformed to polar coordinates,

$$\begin{aligned} H(\mathbf{r}) &= \tan^{-1}(V_2(\mathbf{r})/V_1(\mathbf{r})) \\ S(\mathbf{r}) &= \sqrt{V_1(\mathbf{r})^2 + V_2(\mathbf{r})^2}, \end{aligned} \tag{19}$$

thus obtaining $\mathbf{I}_{IHS}(\mathbf{r}) = (I(\mathbf{r}), H(\mathbf{r}), S(\mathbf{r}))^T$. The hue coordinate range is $[0, 2\pi]$ or, equivalently, $[0, 360]$ degrees.

3.2 Experimental Setup

The data set used in our work consisted of 50 images, natural and man-made/artificial object images. They were collected

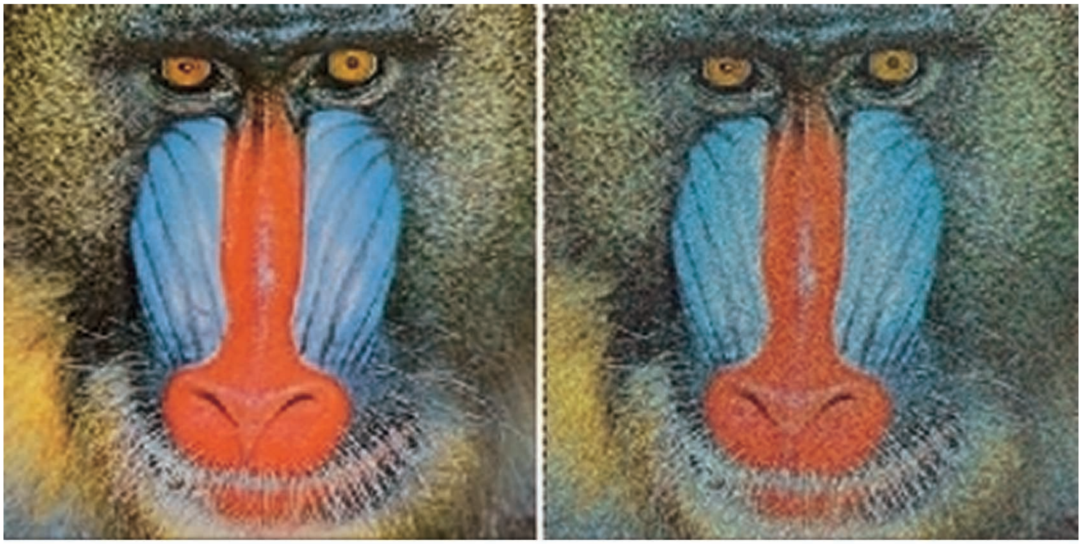

(a) (b)

Fig. 1. (a) The "Mandrill" image and (b) the same image degraded with additive Gaussian noise.

from various sources and do not rely upon any specific acquisition, illumination, resolution, or format constraint. The original images are given in RGB components. In this paper, due to space limitation, we will illustrate results obtained by using the "Mandrill" image (Fig.1a) which is a standard test image and, meanwhile, is particularly critical due to the combination of fine textural features and hue variations.

Equation (9) was implemented using a finite difference form [24]. In order to avoid division by zero, which would occur in (9) when $I_i = 0$, values of $I_i < \epsilon$, where $\epsilon = 1.0^{-5}$ were replaced by $I_i = \epsilon$. In the case of diffusion in IHS space, the angular range of the hue component suggests a careful implementation of (9), as regards gradient computations since, in this case, the finite difference of the values of two pixels, say $H(\mathbf{r})$ and $H(\mathbf{r}')$, cannot be simply computed as $H(\mathbf{r}) - H(\mathbf{r}')$. In fact, for two nearby values on the hue circle (e.g., 360 and 1) the straightforward difference would suggest a maximum distance between two colors that are actually similar. Thus, we adopt the following rule [28]:

$$\text{if } |H(\mathbf{r}) - H(\mathbf{r}')| > H_{\max}/2 \text{ then } dH = H_{\max} - |H(\mathbf{r}) - H(\mathbf{r}')|$$
$$\text{else } dH = |H(\mathbf{r}) - H(\mathbf{r}')| \mathrm{mod}(H_{\max}),$$

where dH denotes the difference $d(H(\mathbf{r}), H(\mathbf{r}'))$ In the general case $H_{\max} = 2\pi$, for practical purposes, we have used scaled values of H and I to the range $[0, 255]$. Note also that this procedure is sufficient for our purposes and we are not considering specific problems related to orientation diffusion which have been investigated in other works [14], [29], but that are out of the scope of this paper.

The two kinds of diffusion were obtained by setting $\chi_{ij} = 0$ for ICD and $0 < \chi_{ij} < 1$ for GSCD. In regards to the latter case, the following values where chosen, based on either prior considerations related to the specific color space and experimental tuning. For RGB space, $\chi_{12} = \chi_{13} = \chi_{23}$, namely, $\chi_{12} = 0.4, \chi_{13} = 0.4, \chi_{23} = 0.4$, because of equal importance of the three channels. CIELAB space separates achromatic and chromatic information and a minor interaction should be allowed between the chromatic channels a^* and b^*, since such interaction gives rise to a mean chromaticity error increasing with χ_{23} (cf. following section); thus, in general, $\chi_{12} = \chi_{13} > \chi_{23}$ and, specifically, $\chi_{12} = 0.7, \chi_{13} = 0.7, \chi_{23} = 0.2$. In regards to the Opponent color space, parameters χ_{ij} should satisfy the condition $\chi_{12} > \chi_{13} > \chi_{23}$; namely, we set $\chi_{12} = 0.7, \chi_{13} = 0.5, \chi_{23} = 0.3$. This constraint allows for a major informational influence of the RG channel with respect to the BY one [17], while ensuring a minor interaction between the two opponents, as opposed to the intensity/chromaticity interaction. For what concerns IHS space, $\chi_{13} > \chi_{12} > \chi_{23}$; such choice endows the saturation channel major informational properties with respect to the hue component. This may seem counterintuitive, at a first sight; however, the rationale stems from the fact—first discussed in [28]—that, if saturation is low, hue is very noisy or unstable, thus conveying irrelevant information; for instance, in determining gradient information, the H channel is in some respect complementary to I and S information. Meanwhile, information exchange between S and H channels, should be limited in order to keep a low-chromaticity error. In the experiments, we use $\chi_{12} = 0.2, \chi_{13} = 0.7, \chi_{23} = 0.1$.

3.3 Experiment I

To evaluate the denoising efficiency of the proposed method, actual images corrupted by Gaussian white noise have been considered, which is a standard experiment in the literature [14], [30], [21].

An example is provided in Fig. 1, where the noisy Mandrill image has been obtained by corrupting each RGB channel with Gaussian noise ($\sigma^2 = 400$). Generalized spatio-chromatic diffusion has then been compared against independent channel diffusion, for each color space previously introduced. The procedure is as follows: 1) transform the noisy RGB image $\widehat{\mathbf{I}}$ into the chosen color space, 2) produce two diffused versions of $\widehat{\mathbf{I}}$ by application both types of diffusion, and, finally, 3) back transform the two diffused images to RGB space. It is worth noting that evaluation in the RGB space after back transformation has the disadvantage of lowering performance, but it

TABLE 1
Denoising Performance

	RGB	CIELAB	Opp	IHS
$\chi_{12}, \chi_{13}, \chi_{23}$	(0.4, 0.4, 0.4)	(0.7, 0.7, 0.2)	(0.7, 0.5, 0.3)	(0.2, 0.7, 0.1)
NSNR (t =10)	14.42 14.01	14.46 15.24	14.42 14.94	14.39 14.96
MCRE (t =10)	6.22 6.24	6.07 5.99	6.25 6.28	6.27 5.82
NSNR (t =30)	13.70 13.44	13.75 14.51	13.70 14.05	13.70 14.18
MCRE (t =30)	6.73 6.52	6.50 6.30	6.75 6.65	6.67 5.83

is more meaningful from a practical standpoint, because, eventually, devices like, for instance, computer screens, produce an RGB image. For objective comparison, two different figures of merit have been adopted, which are standard in the literature [30]. The first measure is the Normalized Signal to Noise Ratio,

$$NSNR = 10 \log_{10}(1/NMSE), \tag{20}$$

where $NMSE = \sum_{\mathbf{r}\in\Omega} \left\| \mathbf{I}(\mathbf{r}) - \mathcal{T}_t \widehat{\mathbf{I}}(\mathbf{r}) \right\|^2 / \sum_{\mathbf{r}\in\Omega} \left\| \mathbf{I}(\mathbf{r}) \right\|^2$ is the normalized mean square error [30], $\mathbf{I}(\cdot)$ and $\mathcal{T}_t \widehat{\mathbf{I}}(\cdot)$ denote the original image vector and the image vector obtained at scale t after diffusion has been performed on the noisy image $\widehat{\mathbf{I}}$. The measurement unit is dB (decibel).

The second measure is the Mean Chromaticity Error defined as the distance between the two points which are the intersection points of $\mathbf{I}(\mathbf{r})$ and $\mathcal{T}_t \widehat{\mathbf{I}}(\mathbf{r})$ with the Maxwell triangle [30]; formally,

$$MCRE = \sum_{\mathbf{r}\in\Omega} \mathcal{C}\left[\mathbf{I}(\mathbf{r}), \mathcal{T}_t \widehat{\mathbf{I}}(\mathbf{r})\right] / |\Omega|, \tag{21}$$

where $\mathcal{C}\left[\mathbf{I}(\mathbf{r}), \mathcal{T}_t \widehat{\mathbf{I}}(\mathbf{r})\right] = \left\| \left(\mathcal{T}_t \widehat{\mathbf{I}}(\mathbf{r}) / \left|\mathcal{T}_t \widehat{\mathbf{I}}(\mathbf{r})\right|\right) - \left(\mathbf{I}(\mathbf{r}) / |\mathbf{I}(\mathbf{r})|\right) \right\|^2$ is the chromaticity error between vectors $\mathbf{I}(\mathbf{r}), \mathcal{T}_t \widehat{\mathbf{I}}(\mathbf{r})$, $\|\cdot\|$ and $|\cdot|$ being the L^2 and L^1 norms, respectively, and $|\Omega|$ the dimension of the image domain Ω. MCRE gives an exact indication of the vectors' divergence from the original directions which can be qualitatively interpreted as the chromaticity error [30]. Results are reported in Table 1, for 10 and 30 iterations of the diffusion process. In each square of Table 1, the number on the top refers to ICD and the other to GSCD; obviously, a better performance is quantified by an higher value of NSNR and a lower value of MCRE.

It should be noted that, with the exception of RGB space, GSCD achieves, in general, better denoising performance with respect to both NSNR and MCRE. In particular, the best performance, as the best trade-off between NSNR and MCRE at increasing iterations, is attained in IHS space (specifically with reference to MCRE). The results of ICD and GSCD can be appreciated in Fig. 2.

In Figs. 3 and 4, magnified details of Mandrill's eyes and whiskers are provided. These examples show that GSCD, in both cases, removes the noise present in the top row images while achieving better preservation of details and semantically important singularities, with respect to ICD.

It is worth pointing out that, given an initial MCRE value of 5.91 for the degraded image $\widehat{\mathbf{I}}$, IHS is the only space in which a lower MCRE is gained by GSCD. Also, MCRE

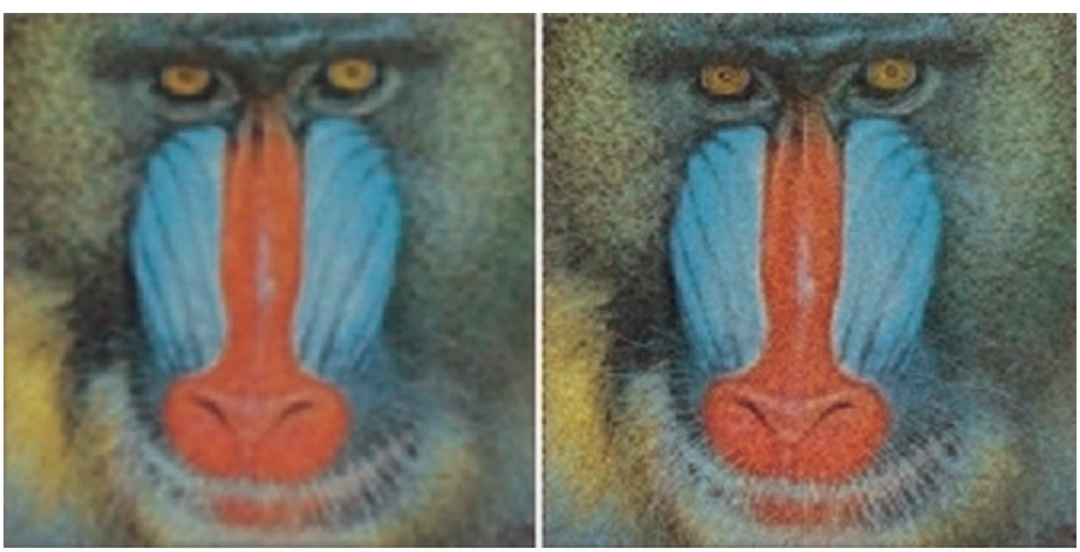

(a) (b)

Fig. 2. The degraded "Mandrill" image after diffusion ($t = 10$) in IHS space: (a) ICD. (b) GSCD.

(a)

(b)

(c)

Fig. 3. (a) Magnified details of the eyes from the degraded image, (b) ICD, and (c) GSCD.

exhibits very low increase when increasing the number of iterations. This result can be partially determined by the setting of the χ parameters, which privileges the S component, consistently with the fact that, in such space, due to the nonlinear transformation from RGB, the noise sensitivity of H component is not homogeneous in the chrominance plane; however, when S is high, H sensitivity to the image noise can be even lower than that of intensity [28]. Eventually, the tuning of the χ_{23} parameter in GSCD allows for a suitable control of the chromaticity error, which is a crucial problem when dealing with color images [30], usually overlooked in other models.

3.4 Experiment II

To provide a qualitative, visual assessment of the two methods for pattern analysis purposes, we have used the outputs of ICD and GSCD at 30 diffusion iterations to perform image segmentation. The same region extraction method was applied to all images. In this case, we used a simple split-and-merge procedure [25] in order to easily control the merge step. Visualization of these results was made easier by an application of Canny's algorithm [31] (with $\sigma = 1$) on each channel's (I_i) segmentation output, so that the colored edge map could be transformed into a gray-scale edge map. It must be emphasized that we have used

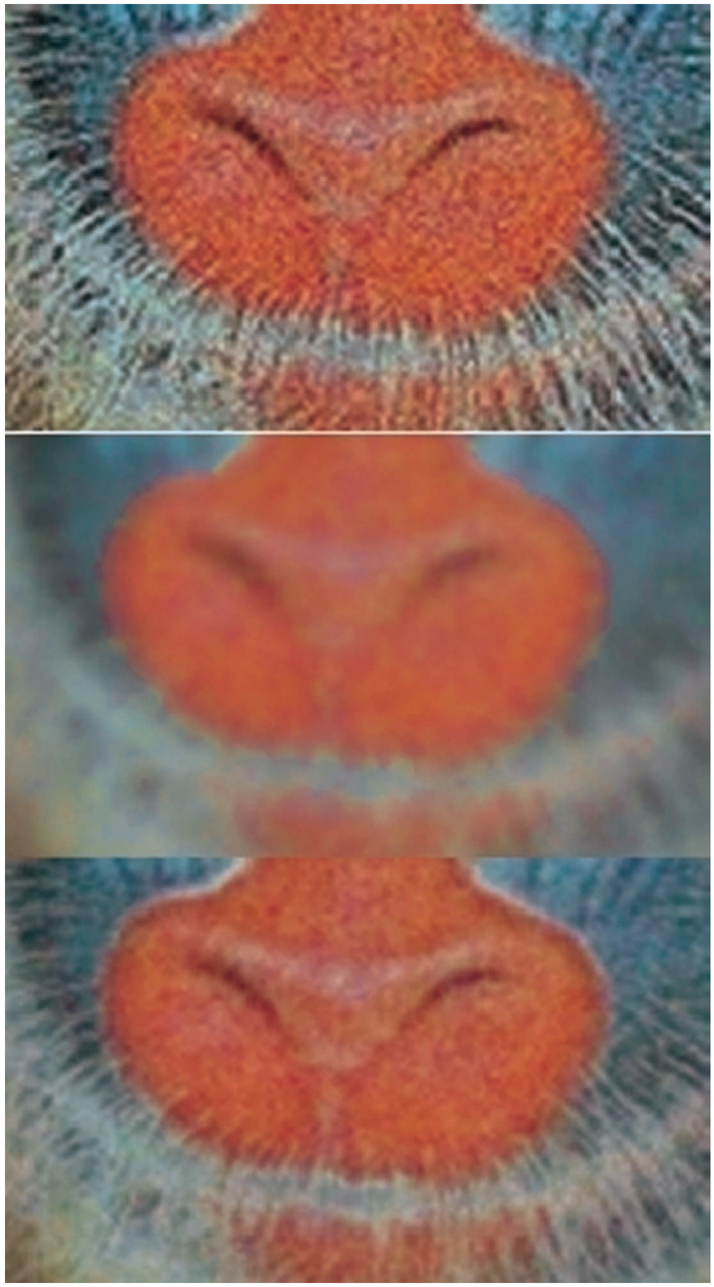

Fig. 4. Magnified details of the nose and whiskers. The organization of the figure is the same as in Fig. 3.

rather simple procedures for segmentation and region boundary identification since they were intended to provide just a simple way to visualize the results yielded by the two diffusion process; the focus here is on the comparison of the two diffusion models and not on segmentation per se. For instance, to effectively address the segmentation issue, a natural choice could be the extension to the proposed framework of entropy-based procedures previously presented in [19], [32]. Indeed, both region extraction and edge detection were run with minimum thresholds to allow for oversegmentation and to visualize better differences between the two diffusion processes. Fig. 5 shows examples in RGB (top row) CIELAB (second row), Opponent (third row), IHS (fourth row) results. In each figure, the left image is obtained after ICD, while the right one after GSCD. Finally, the last row shows IHS segmentation for 100 iterations.

It can be seen that, in general, edge maps obtained after GSCD retain more significant features than those provided by ICD (note, for instance, the right eye of the Mandrill, which is missed by ICD, in CIELAB, Opponent spaces, and IHS at 100 iterations). It is worth remarking that again, for the majority of images of our data set, it is indeed the IHS space which has provided best qualitative results. From the last row of Fig. 5, it is clear that GSCD provides a more stable behavior (in the scale-space sense, [3]) as regards image structures, with respect to ICD.

3.5 Experiment III

One way of quantitatively explaining the differences between the two diffusion models, as regards the results presented

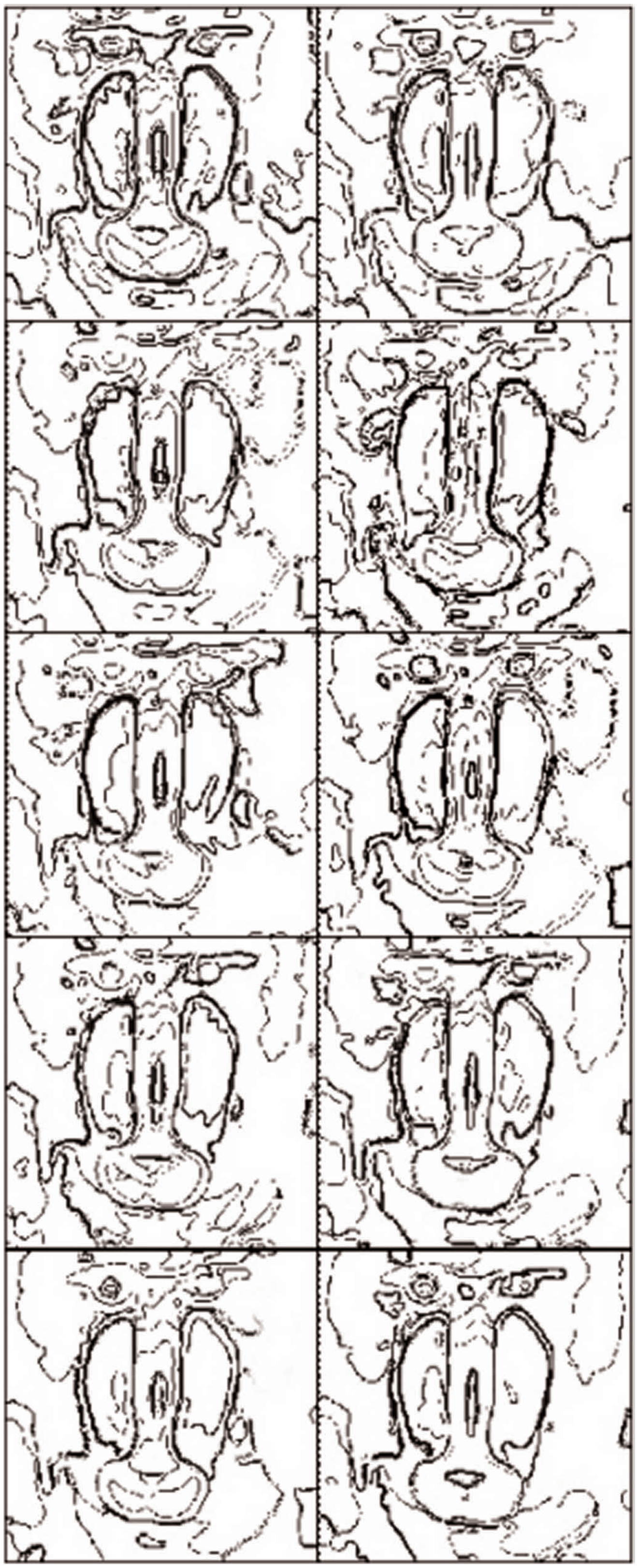

Fig. 5. The figure displays the edge maps images obtained after ICD (left column) and GSCD (right column) for the different color spaces (see text for details).

above, is to measure, for a given image, the total variation along scales of image uniformity with respect to the difference between the original and diffused picture (discrepancy or error). What is obtained is a type of FROC (free receiver operating characteristic) curve where the free parameter is represented by the number of iterations (scales t). Clearly, one expects that, when t increases, the GSCD curve keeps below the ICD curve. In fact, the former type of diffusion should better preserve relevant features (e.g., spatio-chromatic edges) over the different color channels as scale changes, thus allowing less uniformity at a given error/discrepancy level. Formally, define the discrepancy or error E as:

$$E(t) = \sum_{\mathbf{r}\in\Omega} d^2(\mathbf{r},t)/|\Omega|, \tag{22}$$

where $d^2(\mathbf{r},t) = \sum_{i=1}^{m}(I_i(\mathbf{r},t) - I_i(\mathbf{r},0))^2$, $d(\mathbf{r},t)$ being the Euclidean distance of the color vector between the diffused image and the original one of each pixel $\mathbf{r}$ in the domain Ω. By adapting and generalizing to color a uniformity measure previously proposed [33], define

$$U(t) = 1 - \sum_{\mathbf{r}\in\Omega} \bar{\sigma}^2(\mathbf{r},t)/K|\Omega|, \tag{23}$$

where K is a normalization factor, $\bar{\sigma}^2(\mathbf{r},t) = \sum_{i=1}^{m}\sigma_i^2(\mathbf{r},t)$, with

$$\sigma_i^2(\mathbf{r},t) = \sum_{\mathbf{r}\in\mathcal{N}(\mathbf{r})}\left(I_i(\mathbf{r},t) - \mu_{i,\mathcal{N}(\mathbf{r})}(t)\right)^2,$$

$\mathcal{N}(\mathbf{r})$ being a neighborhood of the point $\mathbf{r}$ and $\mu_{i,\mathcal{N}(\mathbf{r})}(t) = \sum_{\mathbf{r}\in\Omega} I_i(\mathbf{r},t)/|\mathcal{N}(\mathbf{r})|$. Fig. 6 shows the plots of $U(t)$ versus $E(t)$ for GSCD and ICD ($t = 30$) in the different color spaces. In general, the area below the curve describing the ICD process is always larger than that one below the GSCD curve. Such difference is greater in CIELAB, Opponent, and IHS spaces than in RGB. In particular, a remarkable difference can be observed for the behavior of IHS, which is rather stable when t increases.

3.6 Experiment IV

The last experiment visualizes some results obtained by implementing the anisotropic extension discussed at the end of Section 2 and formalized through GSCAD equation (13). The results obtained have been compared with results achieved by implementing the PPV method. Fig. 7a shows the Mandrill image after 50 iterations with PPV and Fig. 7b shows GSCAD in RGB space.

We have measured MCRE and NSNR for both images: with a comparable chromaticity error (0.49 for PPV method and 0.44 for GSCAD), GSCAD improves NSNR of about 2 dB (precisely 22.09 dB versus 19.85 dB). In practice, at comparable smoothing capabilities, GSCAD seems somehow to retain better fine details of the image. That can be better appreciated in Fig. 8, which also shows the persistency of this property across scales in that details of mouth and whiskers are preserved in the images obtained after 100 diffusion iterations of both methods.

4 Concluding Remarks

In the framework of open systems thermodynamics, we have proposed an evolution equation based on the assumption that a multivalued image is a complex isolated system, whose

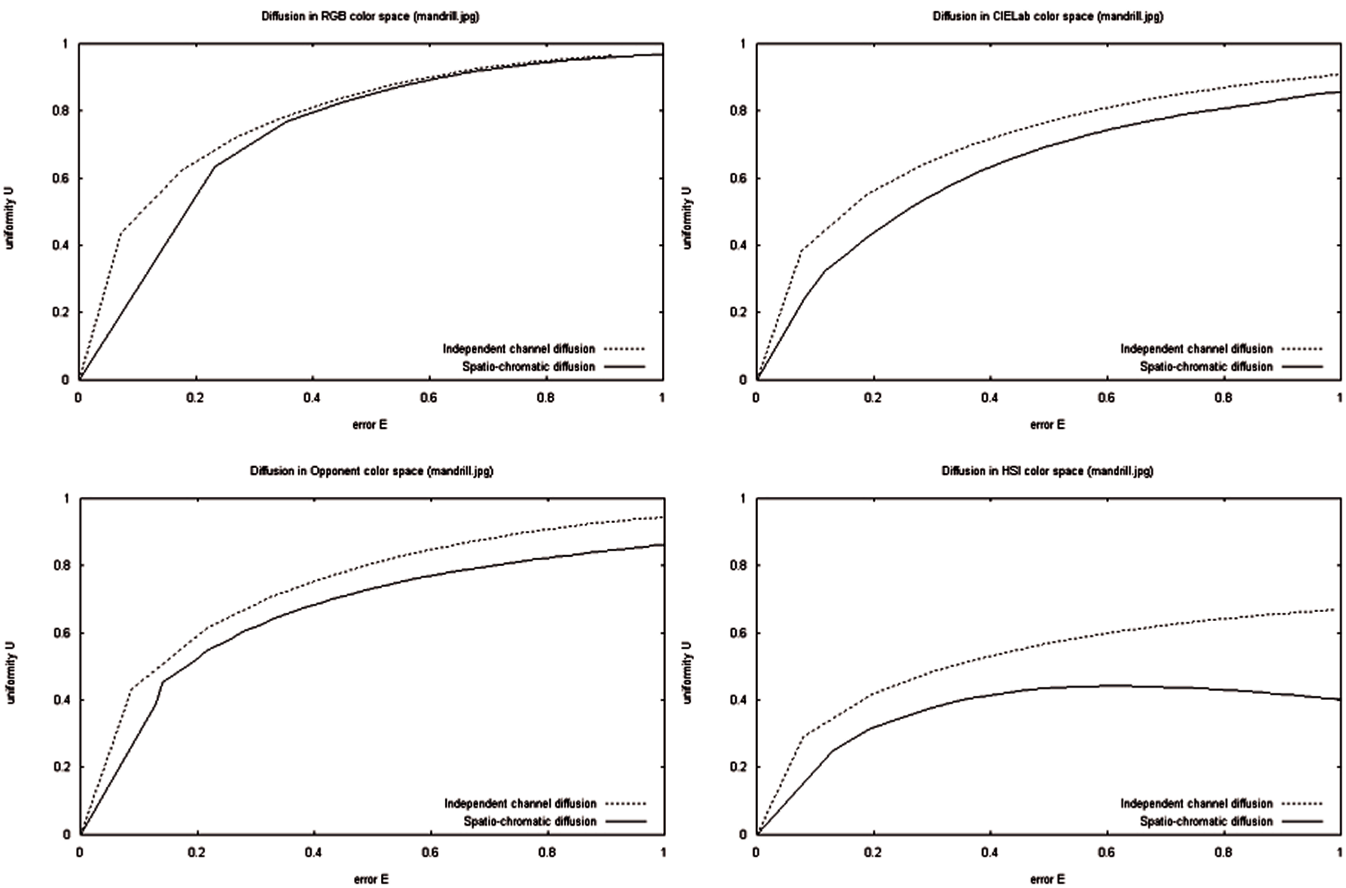

Fig. 6. Uniformity U plotted against error E, as a function of diffusion iterations on the "Mandrill" image in RGB, CIELAB, Opponent, and IHS spaces.

components, namely, the color components, interact with each other through a generalized thermodynamical force. Experiments show that, when the multichannel system evolves in the way we propose and cross-effects between channels are suitably controlled via the χ_{ij} parameters, diffusion takes place while image structures are better retained—and in the absence of any explicit anisotropic biasing.

By taking into account outcomes obtained on our data set, main results achieved can be summarized as follows: 1) GSCD

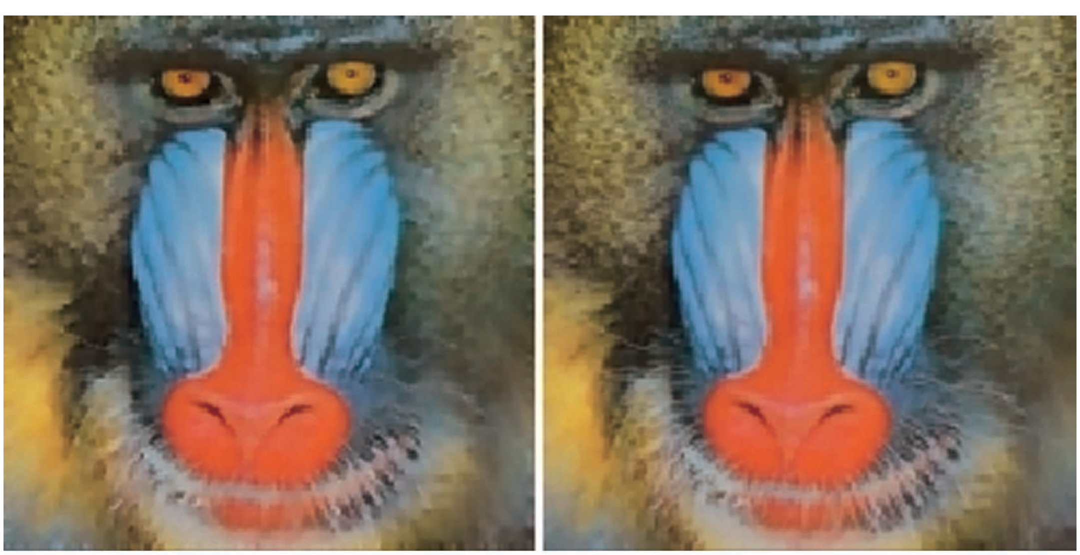

(a) (b)

Fig. 7. (a) Results obtained on the Mandrill image by 50 iterations of the PPV method (b) and GSCAD.

(a)

(b)

Fig. 8. (a) Details of Mandrill's nose and whiskers after 100 iterations of the PPV method and (b) GSCAD.

generally provides a better performance with respect to ICD, in regards to both denoising and image structure preservation, 2) the difference in performance between images is closely related to the amount of background texture, and is less sensible for man-made object images, and 3) using a color space where intensity and chromaticities are represented independently (Opponent, CIELAB, IHS) usually leads to a better behavior of GSCD, provided that parameters χ_{ij} are carefully chosen to modulate interactions between channels; in particular, such effects are remarkable in IHS space, where the complex interplay between saturation and hue is effectively accounted for. From a global point of view, this trend can be quantitatively evaluated via ROC curves.

It is worth remarking that results 2) and 3) are consistent with theoretical and experimental results obtained in [2] and [28]. In general, it can be said that nonlinearities derived in (10) are essential when dealing with vector-valued images as argued by Florack [15]. As concerns comparisons with methods based on anisotropic diffusion our method provide comparable results, with a better signal-to-noise ratio, and, furthermore, it is computationally less expensive.

Most of the discussion provided here refer to color images, which are a special kind of vector-valued image. An interesting extension of this work can be the use of (10) for diffusing higher dimensional vector fields, such as multi-spectral or hyperspectral images. The only requirement is to provide suitable χ_{ij} parameters, so as to mirror the physics of the problem.

The derivation of diffusion equations in the framework of open systems thermodynamics has a potential impact both from the theoretical and experimental standpoints, and can represent a viable alternative to classical or variational approaches to this problem. An example has been given by deriving a simple anisotropic extension of (10). Eventually, the generalization of diffusion to multivalued images conceived in such framework opens an interesting connection with information-theoretic measures based on entropy production, which have been recently proposed for single-valued images [19], [32].

Acknowledgments

The authors are grateful to the referees for their enlightening and valuable comments that have greatly improved the quality and clarity of an earlier version of this paper, and to Francesco Colace for developing PPV code. The paper was also funded by the Italian Ministero per l' Universitá e la Ricerca Scientifica e Tecnologica and by the INFM.

References

[1] B. Dresp and S. Grossberg, "Spatial Facilitation by Colour and Luminance Edges: Boundary, Surface, and Attentional Factors," *Vision Research,* vol. 39, pp. 3431-3443, 1999.

[2] S. Konishi, A. Yuille, J.M. Coughlan, and S. Zhu, "Fundamental Bounds on Edge Detection: An Information Theoretic Evaluation of Different Edge Cues," *Proc. Computer Vision and Pattern Recognition '99,* pp. 573-579, 1999.

[3] A. Witkin, "Scale Space Filtering," *Proc. Int'l Joint Conf. Artificial Intelligence,* pp. 1019-1023, 1983.
[4] J. Koenderink, "The Structure of Images," *Biological Cybernetics,* no. 50, pp. 363-370, 1984.
[5] T. Lindeberg, *Scale-Space Theory in Computer Vision.* Erewhon, NC: His Publisher, 1999.
[6] *Geometry-Driven Diffusion in Computer Vision,* B. ter Haar Romeny, ed., Dordrecht, The Netherlands: Kluwer Academic, 1994.
[7] L. Florack, *Image Structure.* Dordrecht, The Netherlands: Kluwer Academic, 1997.
[8] R. Whitaker and G. Gerig, "Vector-Valued Diffusion," *Geometry-Driven Diffusion in Computer Vision,* B. ter Haar Romeny, ed., Dordrecht, The Netherlands, Kluwer Academic, 1994.
[9] J. Weickert, "Coherence-Enhancing Diffusion of Colour Images," *Proc. Seventh Nat'l Symp. Pattern Recognition and Image Analysis,* vol. 1, pp. 239-244, 1997.
[10] N. Sochen, R. Kimmel, and R. Malladi, "A General Framework for Low Level Vision," *IEEE Trans. Image Processing,* vol. 7, pp. 310-318, Mar. 1998.
[11] G. Sapiro and D. Ringach, "Anisotropic Diffusion of Multivalued Images with Application to Color Filtering," *IEEE Trans. Image Processing,* vol. 5, pp. 1582-1586, Nov. 1996.
[12] J. Weickert, *Anisotropic Diffusion in Image Processing.* Stuttgart, Germany: Teubner Verlag, 1998.
[13] M. Proesmans, E. Pauwels, and L. van Gool, "Coupled Geometry-Driven Diffusion Equations for Low-Level Vision," *Geometry-Driven Diffusion in Computer Vision,* B. ter Haar Romeny, ed., Dordrecht, The Netherlands: Kluwer Academic, 1994.
[14] B. Tang, G. Sapiro, and V. Caselles, "Color Image-Enhancement via Chromaticity Diffusion," *IEEE Trans. Image Processing,* vol. 10, pp. 701-707, May 2001.
[15] L. Florack, "Non-Linear Scale-Spaces Isomorphic to the Linear Case with Application to Scalar, Vector, and Multispectral Images," *J. Math. Imaging and Vision,* vol. 15, pp. 39-53, 2001.
[16] T. Caelli and D. Reye, "On the Classification of Image Regions by Colour, Texture and Shape," *Pattern Recognition,* vol. 26, no. 4, pp. 461-470, 1993.
[17] B. Wandell, *Foundations of Vision.* Sunderland, Mass.: Sinauer, 1995.
[18] S. de Groot and P. Mazur, *Non-Equilibrium Thermodinamics.* Amsterdam: North-Holland, 1962.
[19] M. Ferraro, G. Boccignone, and T. Caelli, "On the Representation of Image Structures via Scale-Space Entropy Condition," *IEEE Trans. Pattern Analysis and Machine Intelligence,* vol. 21, no. 11, pp. 1199-1203, Nov. 1999.
[20] M. Nitzberg and T. Shiota, "Nonlinear Image Filtering with Edge and Corner Enhancement," *IEEE Trans. Pattern Analysis and Machine Intelligence,* vol. 14, pp. 826-833, 1992.
[21] T. Lindeberg and J. Garding, "Shape-Adapted Smoothing in Estimation of 3-D Depth Cues from Affine Distorsions of Local 2-D Brightness Structure," *Proc. Third European Conf. Computer Vision,* vol. 800, pp. 389-400, 1994.
[22] P. Grindrod, *Patterns and Waves.* Oxford, U.K.: Clarendon Press, 1991.
[23] S. Zhu and D. Mumford, "Prior Learning and Gibbs Reaction-Diffusion," *IEEE Trans. Pattern Analysis and Machine Intelligence,* vol. 19, pp. 1236-1250, 1997.
[24] P. Perona and J. Malik, "Scale-Space and Edge Detection Using Anisotropic Diffusion," *IEEE Trans. Pattern Analysis and Machine Intelligence,* vol. 12, pp. 629-639, 1990.
[25] D. Ballard and C. Brown, *Computer Vision.* New York: Prentice Hall, 1982.
[26] G. Wyszecki and W. Stiles, *Color Science-Concepts and Methods, Quantitative Data and Formulas.* New York: Wiley, 1982.
[27] I. Pitas, *Digital Image Processing Algorithms.* London, U.K.: Prentice Hall Int'l, 1993.
[28] T. Carron and P. Lambert, "Color Edge Detector Using Jointly Hue, Saturation and Intensity," *Proc. Int'l Conf. Image Processing '94,* vol. 3, pp. 977-981, Nov. 1994.
[29] P. Perona, "Orientation Diffusions," *IEEE Trans. Image Processing,* vol. 7, pp. 457-467, Mar. 1998.
[30] P. Trahanias and A. Venetsanopoulos, "Vector Directional Filters—A New Class of Multichannel Image Processing Filters," *IEEE Trans. Image Processing,* vol. 2, pp. 528-534, Oct. 1993.
[31] J. Canny, "A Computational Approach to Edge Detection," *IEEE Trans. Pattern Analysis and Machine Intelligence,* vol. 8, no. 6, pp. 34-43, 1986.
[32] G. Boccignone, M. Ferraro, and T. Caelli, "Encoding Visual Information Using Anisotropic Transformations," *IEEE Trans. Pattern Analysis and Machine Intelligence,* vol. 23, no. 2, pp. 207-211, Feb. 2001.
[33] P. Sahoo, S. Soltani, and K. Wong, "A Survey of Thresholding Techniques," *Computer Vision, Graphics, and Image Processing,* vol. 41, pp. 233-260, 1988.

Giuseppe Boccignone received the Laurea degree in theoretical physics from the University of Torino, Italy, in 1985. In 1986, he joined Olivetti Corporate Research, Ivrea, Italy. From 1990 to 1992, he served as a chief researcher of the Computer Vision Lab at CRIAI, Naples, Italy. From 1992 to 1994, he held a research consultant position at Research Labs of Bull HN, Milano, Italy, leading projects on biomedical imaging. In 1994, he joined the Dipartimento di Ingegneria dell'Informazione e Ingegneria Elettrica, University of Salerno, Italy, where he is currently an associate professor of computer science. In 1997, he was appointed research associate at the National Institute for the Physics of Matter (INFM). He has been active in the field of computer vision, image processing and pattern recognition, working on general techniques for image analysis and description, medical imaging, and object-oriented models for image processing. His current research interests include theoretical models for computational vision, active vision, image, and video databases. He is a member of the IEEE and the IEEE Computer Society.

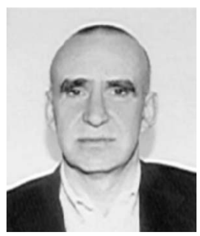

Mario Ferraro received the Laurea degree in theoretical physics from the University of Torino, Italy, in 1973. He has worked in several laboratories in Europe, Canada, and United States, doing research on fuzzy sets theory, human vision, invariant pattern recognition, and computational vision. Presently, he is an associate professor of physics at the University of Torino. His research interests include image and shape analysis, cellular biophysics, and the theory of self-organizing systems.

Terry Caelli received the PhD degree in pattern recognition from the University of Newcastle, NSW, in 1975. His interests lie in computer vision, pattern recognition, and artificial intelligence and their applications to intelligent sensing, image interpretation, the prototyping human perception-action, and human-machine interactions. He is a professor of computing science at the University of Alberta, Canada. He is actively involved as an associate editor of a number of journals in the area and he is a member of several conference organizations. His specific contributions lie in texture processing, invariant pattern/object recognition, and machine learning as applied to spatio-temporal information processing. He has won a number of best paper awards for journal and conference papers and was a recipient of the University of Newcastle Convocation Medal of Excellence, he is a member of the International Association for Pattern Recognition, and a fellow of the IEEE.